p-Type dye-sensitized solar cells based on pseudorotaxane mediated charge-transfer

Bouwens, T.; Mathew, S.; Reek, J.N.H.

DOI
10.1039/c8fd00169c

Publication date
2019

Document Version
Final published version

Published in
Faraday Discussions

Faraday Discussions

Cite this: *Faraday Discuss.*, 2019, **215**, 393

PAPER

p-Type dye-sensitized solar cells based on pseudorotaxane mediated charge-transfer†

Tessel Bouwens, Simon Mathew and Joost N. H. Reek *

Received 7th November 2018, Accepted 23rd January 2019
DOI: 10.1039/c8fd00169c

The efficiency of p-type dye-sensitized solar cells (DSSCs) remains low compared to that of n-type congeners due to charge recombination events. We report a supramolecular approach to reduce recombination at the NiO–dye interface, realized by using the cyclophane cyclobis(paraquat-*p*-phenylene) ring (**RING**$^{4+}$/**RING**$^{3\bullet+}$) as a redox mediator and a dye (**P$_N$**) functionalized with a 1,5-dioxynaphthalene (DNP) recognition site, promoting the supramolecular formation of a pseudorotaxane capable of directing charge transfer away from the NiO–dye interface. The binding affinity of **RING**$^{4+}$ to **P$_N$** is high ($K_{ass} = 3.4 \times 10^4$ M^{-1}), with quenching of the photoexcited dye (**P$_N$***) ascribed to reduction of **RING**$^{4+}$ to **RING**$^{3\bullet+}$. The reduced **RING**$^{3\bullet+}$ exhibits a lower binding affinity to **P$_N$**, facilitating exchange with the excess **RING**$^{4+}$ present in solution. This supramolecular phenomenon was implemented into p-type DSSCs by anchoring the **P$_N$** dye on a NiO photocathode in conjunction with the **RING**$^{4+}$/**RING**$^{3\bullet+}$ redox couple, yielding a 10 fold enhancement in the short-circuit photocurrent (J_{SC}) compared to control devices utilizing **P1** dye or the methylviologen (**MV**$^{2+}$/**MV**$^{\bullet+}$) redox couple that cannot form pseudorotaxanes.

Introduction

Dye-sensitized solar cells (DSSCs), invented by O'Regan & Grätzel in 1991,[1] have complementary advantages to traditional silicon solar cells including low-cost manufacturing,[2] low-light performance,[3] and tunable colors, making them useful for indoor applications and building integrated photovoltaics (BIPV).[4] High-efficiency n-type DSSCs employ sterically demanding dyes and/or surface passivation to shield the TiO_2–electrolyte interface and suppress the recombination of photoinjected electrons.[5,6] This design principle has enabled the use of

Homogeneous Supramolecular and Bio-inspired Catalysis, Van't Hoff Institute for Molecular Sciences (HIMS), University of Amsterdam (UvA), Science Park 904, 1098 XH Amsterdam, The Netherlands. E-mail: j.n.h.reek@uva.nl

† Electronic supplementary information (ESI) available. See DOI: 10.1039/c8fd00169c

alternative redox mediators yielding enhancements of open-circuit voltages (V_{OC}) that translate to power conversion efficiencies (PCEs) beyond 14%.[7,8]

Complementary p-type DSSCs open avenues to tandem solar cells to attain greater PCEs while demonstrating utility for both photovoltaics and solar-driven fuel generation, but they are relatively unexplored compared to their n-type analogue.[9–13] Intrinsic to the operation of p-type DSSCs is electron transfer from the Valence Band (VB) of the p-type semiconductor NiO to the excited state dye (D*).[14,15] However, currently the highest efficiencies of p-type cells are 10 fold lower compared to those of the n-type analogues due to recombination phenomena.[16,17] Electron propagation in p-type DSSCs and recombination phenomena are outlined in Fig. 1. Ideally the absorption of light to generate an excited state dye (D*) will proceed *via* an electron transfer from the VB of NiO (Process 2, Fig. 1) to afford the radical dye anion (D^-). Regeneration of the ground-state dye proceeds *via* a second electron transfer to the redox mediator (Process 3, Fig. 1) allowing the reduced species of the redox couple to diffuse to the counter electrode, regenerate and complete the circuit (Process 4).

Unfavorable recombination phenomena can lower the PCE by creating competition for the forward electron transfer to the redox couple.[18,19] Ultra-fast recombination between the radical dye anion and the hole in the VB of NiO (Process 6, Fig. 1) is ameliorated by the molecular engineering of donor–π–acceptor dyes. Spatial separation of the donor near the semiconductor surface and the acceptor away from the NiO surface promotes vectorial electron transfer away from the surface upon light absorption, increasing the lifetime of the photoreduced excited state.[20–22] The second recombination process involves the electron transfer from the reduced redox couple to the VB of the NiO (Process 5, Fig. 1). As charge migration is relatively slow in NiO (4×10^{-8} cm^2 s^{-1}), this process also significantly contributes to the low efficiencies.[23]

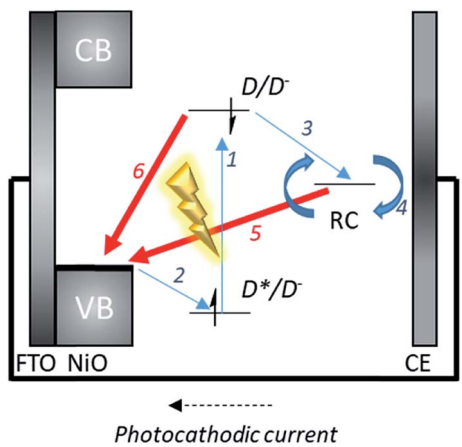

Fig. 1 A schematic representation of a p-type DSSC. The blue arrows represent the forward electron propagation processes and the red arrows show the unfavorable recombination phenomena. FTO = Fluorine Tin Oxide. RC = Redox Couple. CB = Conduction Band. VB = Valence Band. D = Dye. D* = excited state dye. D^- = radical dye anion.

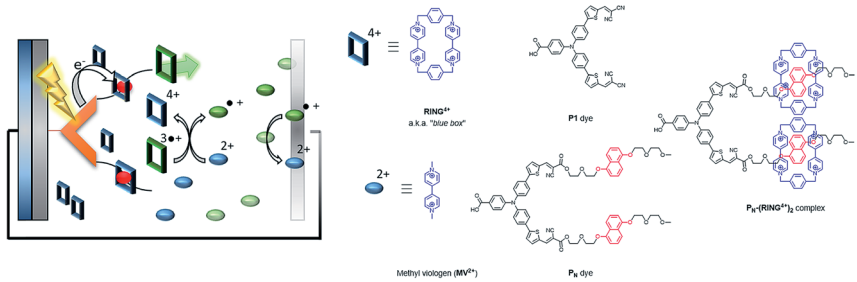

Fig. 2 The proposed operational principle of the pseudorotaxane-based p-type DSSC. The ring in the oxidized form ($RING^{4+}$, blue) has a high affinity for the binding site (DNP, in red) in contrast to the reduced ring ($RING^{3\bullet+}$, green), leading to a high local concentration of $RING^{4+}$ close to the dye. The molecular structures of P_N, **P1**, the ring $RING^{4+}$, MV^{2+} and the P_N–$(RING^{4+})_2$ complex (right).

With these challenges in mind, we propose a novel approach to the construction of a p-type DSSC in which we functionalize the dye with a 1,5-dioxynaphthalene (DNP) recognition site for the ring to form a pseudorotaxane with the cyclophane cyclobis(paraquat-*p*-phenylene) ring, $\mathbf{RING^{4+}}$, being the oxidized form of the redox couple.[24] Electron transfer from D^- reduces $\mathbf{RING^{4+}}$, yielding $\mathbf{RING^{3\bullet+}}$ which loses affinity for the recognition site and is driven away from the dye–semiconductor interface, facilitating charge rectification within the device (Fig. 2).

This self-assembly strategy is unknown for p-type cells based on the I^-/I_3^- redox couple.[25] Pre-organization of the redox couple should result in improving the competitiveness of forward electron propagation in the device compared to charge recombination. This is in contrast to the operation of current liquid DSSCs where the electron transfer between the dye and redox mediator is dictated by diffusion (collisional) phenomena.

In this paper we report the synthesis of dyes with recognition sites that facilitate pseudorotaxane formation and implementation into a p-type DSSC where the ring acts as a redox mediator. Initial experiments confirm that this supramolecular approach results in a ~10 fold improvement in photocurrent compared to that of control cells without supramolecular motifs for pre-organization.

Results and discussion

Design and description of the components

Creating a switchable pseudorotaxane-based DSSC requires the components to meet specific criteria. Firstly, the oxidized form of the ring component in the pseudorotaxane must have a high affinity (high binding constant, K_{ass}) for the recognition site, accompanied by a decrease in K_{ass} upon reduction of the ring, facilitating ring exchange and charge transport. Secondly, the redox potentials of all of the components must promote forward electron propagation by an electron cascade triggered by the absorption of light to reduce the ring as the redox mediator. With these requirements in mind, we considered pseudorotaxanes developed by Stoddart and coworkers as suitable.[24,26] The electron-deficient ring

structure **RING**$^{4+}$, or the famous "blue box", exhibits a strong electrostatic interaction with the electron rich DNP (Fig. 2, in red).[27] Upon reduction of **RING**$^{4+}$ to **RING**$^{3\bullet+}$ *via* chemical,[28] electrochemical[29] or photochemical stimuli,[30,31] the increase in electron density causes a loss of affinity for the DNP recognition site.[26,32]

We decided to modify the **P1** dye system[20,33] as it can accommodate the incorporation of the DNP recognition sites at the acceptor part with minimal perturbation of the dye electronic structure (Fig. 2) so that the energy levels of the NiO VB, the dye and the redox couple match to allow for forward electron propagation within the system (Fig. 3). Initial experiments showed that high concentrations of the ring caused detachment of the $\mathbf{P_N}$ dye, a problem that was solved by using low concentrations of **RING**$^{4+}$ and **MV**$^{2+}$ as the main redox mediator as the former is essentially two connected **MV**$^{2+}$ molecules.

Synthesis of the building blocks

The **P1** dye[20] and the [**RING**·**4PF$_6$**][34] were prepared according to literature procedures. The $\mathbf{P_N}$ dye functionalized with the DNP recognition site was prepared using a modified procedure, outlined in Scheme 1. The bisaldehyde **4** was reacted with malononitrile to obtain **P1**.[20] The last step in the preparation of $\mathbf{P_N}$ involves a Knoevenagel condensation of **4** with the cyanoacrylate-functionalized DNP unit **1**. After purification by column chromatography the $\mathbf{P_N}$ dye was obtained as a waxy red solid in 11% yield. The compound was comprehensively characterized by ^{1}H NMR, ^{13}C NMR, FD-MS, ATR-IR, CV, and UV-vis.

Optical and electrochemical properties

The absorption maxima and electrochemical properties of **P1** and $\mathbf{P_N}$ are presented in Fig. 4 and summarized in Table 1. A strong absorption between 400–680 nm was ascribed to intramolecular charge transfer, with the maximum for $\mathbf{P_N}$

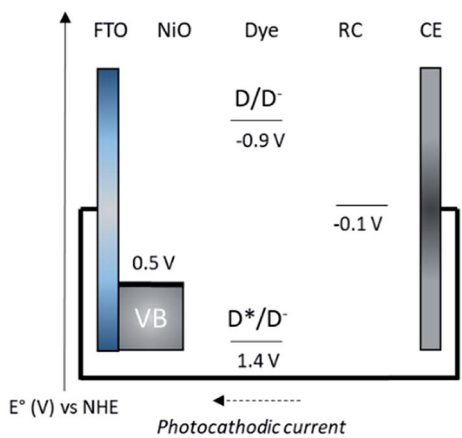

Fig. 3 A schematic energy diagram for the p-type DSSC based on the $\mathrm{P_N}$ pseudorotaxane dye. Energy levels are represented in *V versus* NHE. This effectively creates a local high concentration of oxidized redox mediator in close proximity to the dye, facilitating the productive transfer processes compared to recombination pathways.

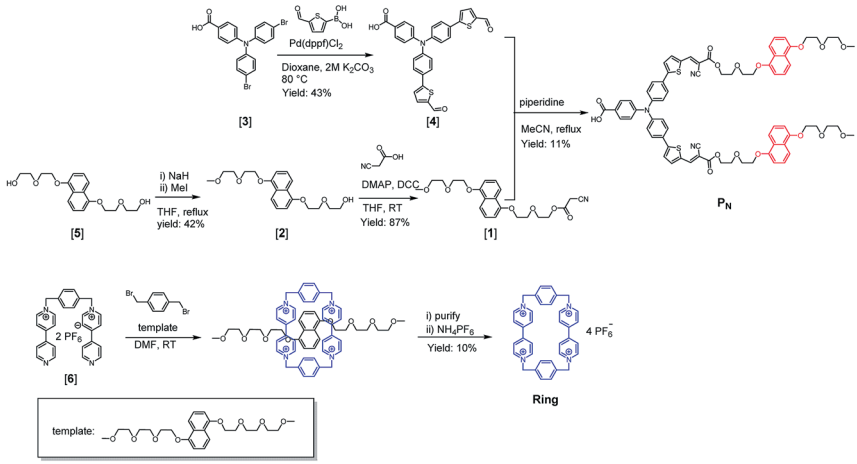

Scheme 1 Synthesis of P_N dye with DNP recognition sites and synthesis of the ring.

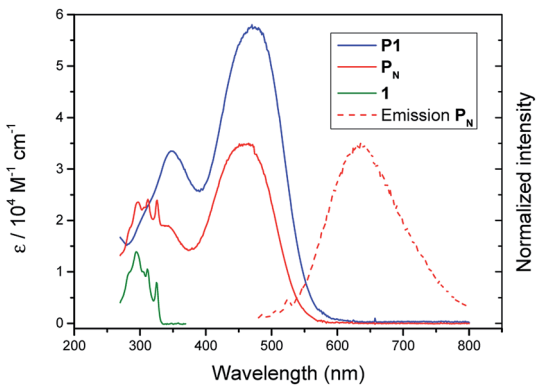

Fig. 4 UV-vis spectra of **P1** (solid blue line), P_N (solid red line) and compound **1** (solid green line) together with the normalized emission spectrum of P_N upon excitation at 450 nm (dashed red line).

(450 nm) slightly blue-shifted in comparison to that for **P1** (475 nm). This blue shift arises from the slight difference in electron withdrawing capability of the acceptor due to the substitution of one cyano group with an ester. The absorption of the DNP unit is a clearly visible feature between 270–340 nm in the UV-vis spectrum of the P_N dye, and the absorption spectrum of P_N indeed approximates a superposition of the UV-vis spectra of both compound **1** and **P1** (Fig. 4). Furthermore, the DNP unit in P_N exhibits a structured fluorescence band with a maximum at 344 nm upon excitation at 310 nm, while the dye part of P_N shows a broad fluorescence feature at 630 nm upon excitation at 450 nm as is shown in Fig. 4. There is no electronic communication between the DNP group and the dye part of P_N as these fluorescence features are separated from each other and only appear upon excitation at 310 nm or 450 nm, respectively.

Table 1 Optical and electrochemical properties of **P1** and $\mathbf{P_N}$ (0.5 mM) in MeCN. The redox potentials were determined in 0.1 M $TBAPF_6$ with a glassy carbon working electrode, a leakless Ag/AgCl reference electrode and a Pt wire as the counter electrode

Dye	λ_{max} (nm)	ε (L mol^{-1} cm^{-1})	$E_{0\text{-}0}$ (eV)	$E_{(D^+/D)}$ (*V vs.* NHE)	$E_{(D/D^-)}$ (*V vs.* NHE)
P1	485	5.8×10^4	2.27	1.30	−0.67
$\mathbf{P_N}$	450	3.5×10^4	2.30	1.32	−0.98

NMR investigation of binding phenomena

The binding of $\mathbf{RING^{4+}}$ to the $\mathbf{P_N}$ dye is qualitatively confirmed by a 5 point ^{1}H NMR titration (Fig. S13†). Mixing of the components resulted in an upfield shift for the resonances originating from $\mathbf{RING^{4+}}$ ($\delta = 0.02$ ppm) and the DNP ($\delta = 0.20$ ppm) moiety with concomitant peak broadening observed in the ^{1}H NMR spectra. DOSY NMR (Fig. S14†) established that both the $\mathbf{P_N}$ dye and $\mathbf{RING^{4+}}$ components in the $\mathbf{P_N}$–$\mathbf{RING^{4+}}$ complex demonstrate identical diffusion constants (5.50×10^{-10} m^2 s^{-1}) that are slightly smaller than that of the $\mathbf{P_N}$ dye (1.02×10^{-9} m^2 s^{-1}) and significantly smaller than that of $\mathbf{RING^{4+}}$ (1.26×10^{-10} m^2 s^{-1}). This observation is consistent with the $\mathbf{P_N}$–$\mathbf{RING^{4+}}$ complex exhibiting rigidification upon complex formation at the DNP recognition site, manifesting in an increase in the hydrodynamic radius. Quantification of the binding constant (K_{ass}), along with the photoinduced charge transfer in the $\mathbf{P_N}$–$\mathbf{(RING^{4+})_2}$ complexes, was investigated by fluorescence quenching studies.

Fluorescence quenching studies

The K_{ass} of $\mathbf{RING^{4+}}$ to the $\mathbf{P_N}$ dye was measured by titration, monitoring the quenching of emission from the DNP moiety in $\mathbf{P_N}$ ($l_{em} = 344$ nm) upon the addition of aliquots of $\mathbf{RING^{4+}}$.[35] The K_{ass} obtained by fitting the titration curve using a Host–Guest–Guest (HGG) model, as introduced by Hunter[36] showed that binding of $\mathbf{RING^{4+}}$ to the two binding sites exhibited almost the same association constant ($K_{ass} = 3.4 \times 10^4$ M^{-1}). The cooperativity factor α is determined to be 0.7, suggesting a minor negative cooperativity, *i.e.* the first binding event for the formation of $\mathbf{P_N}$–$\mathbf{(RING^{4+})}$ is slightly stronger than the second binding event to form $\mathbf{P_N}$–$\mathbf{(RING^{4+})_2}$. Overall the association constant is of the same order of magnitude as was previously reported for a related system.[37]

Next, it was investigated whether the ring is able to quench the excited state of the dye when bound to the DNP recognition site. Upon formation of the $\mathbf{P_N}$–$\mathbf{(RING^{4+})_2}$ complex, 83% of the fluorescence of the dye at 630 nm was quenched. No other emission was observed, which is in line with a photoinduced electron transfer process.

Photovoltaic properties

The NiO working electrodes were functionalized with sensitizers by soaking the electrodes in dye solution (**P1** or $\mathbf{P_N}$ in MeCN) for 16 hours. Adsorption of the dye was confirmed by the loss of the $\nu_{C=O}$ bands of the acidic group of the dye in the ATR-IR spectra (Fig. S8†). Dye desorption experiments show that the dye coverage is 1.6×10^{-8} mol cm^{-2} for $\mathbf{P_N}$. To prove the effect of pseudorotaxane-mediated

pre-organization, $\mathbf{MV}^{2+}$ on its own as the electrolyte was employed as the control for $\mathbf{RING}^{4+}$. They both demonstrate similar reduction potentials (Table S3†), differing in their ability to participate in pseudorotaxane formation, *i.e.* $\mathbf{MV}^{2+}$ is not able to form a pseudorotaxane whereas $\mathbf{RING}^{4+}$ is.[38,39] DSSCs employing four different combinations of dye (either **P1** or $\mathbf{P_N}$) and redox couple (either 25 mM $\mathbf{MV}^{2+/\bullet+}$ or 24.925 mM $\mathbf{MV}^{2+/\bullet+}$ with 75 μM (0.3 mol%) $\mathbf{RING}^{4+/\bullet3+}$) were fabricated. This relatively low concentration of $\mathbf{RING}^{4+}$ is used in the cell as initial experiments revealed that the use of 25 mM (*i.e.* 100%) $\mathbf{RING}^{4+/3\bullet+}$ as the electrolyte results in leaching of the $\mathbf{P_N}$ dye from the surface, observed as the sensitized orange color of the photocathode disappearing upon introduction of the electrolyte (for further explanation see ESI 8†). The redox couple was added as a mixture of the reduced and non-reduced species (*i.e.* $\mathbf{MV}^{\bullet+} : \mathbf{MV}^{2+} = 9 : 1$) by combining a pre-reduced 25 mM $\mathbf{MV}^{\bullet+}$ solution with a non-reduced 25 mM $\mathbf{MV}^{2+}$ solution. As the reduced electrolyte containing $\mathbf{MV}^{\bullet+}$ and $\mathbf{RING}^{3\bullet+}$ is sensitive to oxygen, all of the DSSCs were constructed under inert atmosphere inside a nitrogen filled glovebox. The properties of the DSSCs were measured directly after fabrication in a two-electrode system, connected to a potentiostat to measure the Short-Circuit photocurrent density J_{SC} (*i.e.* at zero bias) under AM1.5 G illumination (100 mW cm^{-2}) in 30 second cycles (Fig. 5), with the data summarized in Table 2.

The DSSCs based on the **P1** and the $\mathbf{P_N}$ dye with $\mathbf{MV}^{2+/\bullet+}$ as the electrolyte (Entry 1 and 2) give identical photocurrents, indicating that the new $\mathbf{P_N}$ dye functions similarly to the known **P1** dye in this set-up. Entry 2 shows that, in the presence of $\mathbf{RING}^{4+/\bullet3+}$ and in the absence of the recognition site, similar currents to those in Entry 1 and 3 are observed. Only DSSCs utilizing the $\mathbf{P_N}$ dye and the $\mathbf{RING}^{4+/\bullet3+}$ redox mediator elements, conducive to pseudorotaxane formation, exhibit a dramatic increase in photocurrent (Entry 4). In addition the photocurrent profile features an initial spike at −17 μA cm^{-2} which decays down to a constant

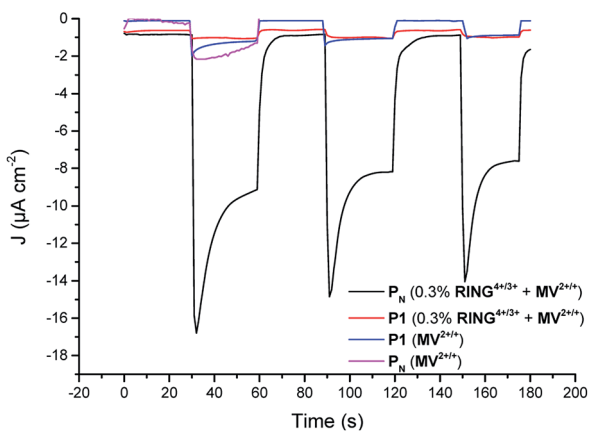

Fig. 5 The photocurrents obtained by switching the solar simulator on and off in cycles of 30 seconds connected to a potentiostat to measure the photocurrent at zero bias under AM1.5 G illumination (100 mW cm^{-2}). The black line ($\mathbf{P_N}$ with 75 μM 0.3 mol% $\mathbf{RING}^{4+}$ and 24.925 mM $\mathbf{MV}^{2+/\bullet+}$) indicates 10 times more photocurrent than the pink line ($\mathbf{P_N}$ with 25 mM $\mathbf{MV}^{2+/\bullet+}$), the red line (**P1** 75 μM 0.3 mol% $\mathbf{RING}^{4+}$ and 24.925 mM $\mathbf{MV}^{2+/\bullet+}$) and the blue line (**P1** with 25 mM $\mathbf{MV}^{2+/\bullet+}$).

Table 2 Obtained J_{SC} values for the four different constructed DSSCs

Entry	Dye	Redox couple	J_{SC} (μA cm^{-2})
1	**P1**	$\mathbf{MV}^{2+/\cdot+}$ only	−1.31
2	**P1**	0.3% $\mathbf{RING}^{4+}$ + $\mathbf{MV}^{2+/\cdot+}$	−1.02
3	$\mathbf{P_N}$	$\mathbf{MV}^{2+/\cdot+}$ only	−1.41
4	$\mathbf{P_N}$	0.3% $\mathbf{RING}^{4+}$ + $\mathbf{MV}^{2+/\cdot+}$	−9.56

value of −9.56 μA cm^{-2}, indicative of a mass transport limitation as the diffusion of $\mathbf{MV}^{2+/\cdot+}$ to the counter electrode is slower than the I^-/I_3^- redox couple due to its larger molecular size. This is a well-known phenomenon in n-type DSSC with redox couples based on larger molecules than the I^-/I_3^- redox couple.[40,41]

Although the photocurrents are low for the control DSSC, in these experiments the typical spike phenomenon is also observed (Fig. 5). These initial experiments demonstrate that the presence of a recognition site, enabling pre-organization of an electron acceptor by pseudorotaxane formation that also acts as a redox couple, leads to DSSCs exhibiting higher photocurrents. This suggests that the pseudorotaxane approach may indeed be a useful strategy to reduce charge recombination in p-type DSSCs.

Conclusions

We proposed here a new type of p-type DSSC where the redox acceptor is pre-organized to the dye, directing charge transfer away from the dye–electrolyte interface. We constructed a new dye, $\mathbf{P_N}$, based on the previously reported **P1** dye, functionalized with DNP moieties that can form pseudorotaxanes with the electron acceptor $\mathbf{RING}^{4+}$, providing competition with recombination by directing charge transfer away from the dye. $\mathbf{RING}^{4+}$ shows a high binding affinity (3.4×10^4 M^{-1}) for the DNP recognition sites installed on the $\mathbf{P_N}$ dye and the affinity for the reduced ring $\mathbf{RING}^{3\cdot+}$ is known to be low. Implementation into p-type DSSCs showed that pseudorotaxane formation afforded photocurrents almost one order of magnitude higher than those of the control experiments. Future research will be focused on time-resolved characterization of the system to provide quantification of reductions in charge recombination. Also, as the eventual efficiencies of the fabricated DSSCs are still rather low, we aim to further improve this using the concept introduced in this paper.

Material and instruments

All of the reagents and solvents were obtained from Sigma-Aldrich, Fluorochem and VWR, and were used without purification. Compound **3** was obtained following a literature procedure.[20] MeCN and THF were dried in a solvent purification system. Column chromatography was performed using silica gel (SiliCycle, SiliaFlash P_{60}, 40–63 μm, 230–400 mesh) while fractions were analyzed using TLC (TLC silica gel 60 F_{254} from Merck KGaA) visualized with 254/350 nm light. The products were analyzed using MS, NMR and IR. ^{1}H-NMR and ^{13}C NMR spectra were recorded on a Bruker AV300 and AV400 spectrometer and are reported in ppm using a solvent residual signal as an internal standard (7.26 ppm

for $CDCl_3$ and 2.05 ppm for $(CD_3)_2CO$). 2D ^{1}H-DOSY spectral data were acquired with temperature and magnetic gradient calibration prior to the measurements, and the temperature was kept at 298 K during the measurements. IR spectra were recorded on a Bruker Alpha FTIR machine. The exact mass of the compounds was obtained on an AccuTOF GC v 4g, JMS-T100GCV Mass spectrometer (JEOL, Japan) equipped with an FD Emitter, Carbotec or Linden (Germany), FD 13 μm. The current rate was 51.2 mA min^{-1} over 1.2 min *via* a machine using field desorption (FD) as the ionization method. UV-vis measurements were performed on a single beam Hewlett Packard 8453 spectrometer in a 10 mm path length quartz cuvette using MeCN as the background. (Photo)electrochemical experiments were performed with a g-stat potentiostat from Autolab and an Oriel LCS-100 solar simulator. The light intensity was set to 100 mW cm^{-2} *via* a calibrated DSSC Newport, 91150-2000. Fluorescence spectra were recorded on a Fluorolog Jobin Yvon-SPEX together with their corresponding UV-vis spectra (Shimadzu UV-2700 Spectrophotometer).

Dye-sensitized solar cell fabrication and characterization

The NiO was bought as a paste (Ni-Nanoxide N/SP from Solaronix) and screen printed on FTO glass obtained from Sigma Aldrich (2.2 mm, 7 Ω/sq) as 0.5 cm diameter circles. Sandwich cells were constructed with carbon based counter electrodes separated from the working electrode using Meltonix polymer 1170-60 (Solaronix, Switzerland) with a thickness of 60 μm. The preparation of electrolyte and the DSSCs was performed under inert atmosphere (N_2) in a glovebox since the reduced species $\mathbf{MV}^{\bullet+}$ and $\mathbf{RING}^{3\bullet+}$ are reactive towards oxygen. The reduced $\mathbf{MV}^{\bullet+}$ was prepared by the addition of Zn dust (2 equiv.) to a 25 mM solution of $\mathbf{MV}^{2+}$ in 1 M LiTFSI as the supporting electrolyte in N_2 degassed MeCN. Reduction is clearly visible as the color changes from colorless to dark blue. After stirring for 1 hour, the final electrolyte solution was prepared by adding 9 parts filtered reduced solution with 1 part oxidized $\mathbf{MV}^{2+}$, both 25 mM (either with 25 mM $\mathbf{MV}^{2+}$ or 24.925 mM $\mathbf{MV}^{2+}$ with 75 μM (0.3 mol%) $\mathbf{RING}^{4+}$). Filtration of the reduced solution is required to remove excess Zn dust and precipitated Zn^{2+}. Then the electrolyte was introduced inside the cells *via* a pre-drilled hole. After cleaning and wiping the outside of the cell, the hole was sealed with the Meltonix polymer and optical glass plate by melting the polymer using a 350 °C heating source. The DSSCs were measured directly after fabrication using a g-stat potentiostat and solar simulator. The cells were masked to make sure 0.126 cm^2 of the NiO surface was irradiated, to stay consistent throughout all of the measurements.

Electrochemistry

Cyclic voltammograms and differential pulse voltammograms were recorded on a potentiostat PGSTAT302N from Autolab with a glassy carbon working electrode (MetrOhm, diameter 3 mm), a leakless Ag/AgCl reference electrode (eDAQ, ET069) and a Pt wire as the counter electrode. The analyte solution was prepared by degassing a 100 mM $TBAPF_6$ solution with N_2 and adding this to the analyte to obtain a 0.5 mM final analyte solution.

Binding studies

In order to determine the K_{ass} of the ring to the dye, a solution of $\mathbf{P_N}$ was kept at a constant concentration (5 μM) and titrated with an increasing concentration of ring (2 mM and 10 mM) inside a fluorescence cuvette with a path length of 10 mm. After each addition of the ring the fluorescence at 344 nm was recorded by irradiation with 310 nm light and the UV-vis spectrum was measured to correct for the inner-filter effect following the formula described by Turner and coworkers:[42]

$$F_{corr} = F_{obs} \times 10^{\left(\frac{A_{exc}+A_{emm}}{2}\right)}$$

The corrected data was fitted to a 1 : 2 host–guest model using a Matlab script.[43]

Excited state quenching studies

The excited state quenching studies were performed using a similar approach to that of the determination of K_{ass}. The $\mathbf{P_N}$ was kept at a constant concentration (10 μM) and was titrated with an increasing concentration of ring (4 mM and 20 mM). The decrease in the fluorescence at 630 nm upon excitation with 450 nm light was directly used to determine the amount of quenching and no correction was needed as there was no self-absorption of the sample at 630 nm.

Synthesis

Compound 2. To a solution of compound **5** (2.00 g; 5.94 mmol; 1 equiv.) in dry THF (15 mL), NaH (242.6 g; 6.06 mmol; 1.02 equiv.) in mineral oil (65%) was added portion wise. Upon addition, a precipitate was formed and a gas was released. After the mixture was heated at reflux for 1 hour, MeI (614 mg; 268 μL; 7.13 mmol; 1.2 equiv.) was added all at once. After heating at reflux for 4 more hours the reaction mixture was quenched by the dropwise addition of water. The water layer was extracted with EtOAc (3×). The combined organic layers were dried with Na_2SO_4. After filtering of the Na_2SO_4 the organic solvents were evaporated. The product was purified by column chromatography (silica, DCM/EtOAc, 1 : 1, the second fraction). Compound **2** was obtained as a yellow oil. Yield: 875 mg (42%). The ^{1}H-NMR was consistent with the literature.[39]

Compound 1. Compound **2** (825 mg; 2.35 mmol; 1 equiv.), cyanoacetic acid (210.3 mg; 2.47 mmol; 1.05 equiv.) and a pinch of DMAP were dissolved in 10 mL of dry DCM. DCC (510 mg; 2.47 mmol; 1.05 equiv.) was added and direct precipitation of DCU was observed upon addition. After stirring overnight at RT, DCU was filtered of and DCM was removed and the crude was purified by column chromatography (silica, DCM/EtOAc, 4 : 1). Compound **1** was obtained as an off-white waxy solid. Yield: 854 mg (87%). ^{1}H NMR (400 MHz, $CDCl_3$) δ 7.85 (dd, J = 19.5, 8.5 Hz, 2H), 7.35 (td, J = 8.0, 4.1 Hz, 2H), 6.83 (dd, J = 7.6, 4.4 Hz, 2H), 4.39–4.33 (m, 2H), 4.28 (dt, J = 9.8, 4.8 Hz, 4H), 3.97 (dt, J = 11.7, 4.7 Hz, 4H), 3.87–3.74 (m, 4H), 3.62–3.55 (m, 2H), 3.39 (d, J = 4.4 Hz, 5H). ^{13}C NMR (75 MHz, $CDCl_3$) δ 162.99, 154.40, 154.18, 126.80, 126.71, 125.24, 125.06, 114.84, 114.38, 112.85, 105.76, 105.74, 77.23, 72.03, 70.89, 69.86, 69.46, 68.84, 67.93, 65.82, 63.64, 59.10, 24.61. IR ν_{max} (cm^{-1}) 2924 (b, –CH_2– glycol), 2226 (w, CN),

1749 (s, C=O). FD-MS (in MeCN) *m*/*z*: calculated for $C_{22}H_{27}N_1O_7$ $[M]^+$: 417.1788. Found 417.1808.

Compound 4. To a mixture of compound **3** (140 mg; 0.31 mmol; 1 equiv.) and boronic acid (195 mg; 1.25 mmol; 4 equiv.) in dioxane (28 mL), 3.5 mL of 2 M K_2CO_3 in water was added. The mixture was degassed with N_2 for one hour before the Pd(dppf)Cl_2 catalyst (42 mg 0.05 mmol; 15 mol%) was added. The mixture was stirred at 80 °C overnight. The dioxane was removed and water was added. The water layer was acidified to approximately pH 3 after which the water layer was extracted with EtOAc. The organic layers were combined and dried with Na_2SO_4. After filtration the EtOAc was evaporated. The crude mixture was purified by column chromatography (silica, DCM/MeOH/acetic acid, 98% : 2% : 0.002%). Yield: 67.9 mg (43%). The ^{1}H NMR spectrum corresponds to the literature.[20]

P_N dye. Compound **1** (189 mg; 0.45 mmol; 3.5 equiv.), compound **4** (66 mg; 0.13 mmol; 1 equiv.) and 4 drops of piperidine were dissolved in MeCN (22 mL) and heated at reflux for 4 hours. The MeCN was evaporated and acidified water was added (pH 3.5). The organic compounds were extracted with DCM. After drying the organic layers with Na_2SO_4 and filtration, the product was purified by column chromatography (silica, DCM/MeOH/acetic acid, 98% : 2% : 0.002%). The red fractions containing product were checked for their purity by MS and pure fractions were combined to yield the product **P_N** as a waxy, red solid. Yield: 18.7 mg (11%). ^{1}H NMR (300 MHz, $(CD_3)_2CO$) δ 8.21 (s, 2H) 8.01 (d, J = 8.4 Hz, 2H), 7.85 (t, J = 8.7 Hz, 4H), 7.63 (t, J = 6.8 Hz, 6H), 7.34 (dd, J = 9.4, 6.3 Hz, 6H), 7.17 (dd, J = 14.1, 8.4 Hz, 6H), 6.83 (dd, J = 19.8, 7.7 Hz, 4H), 4.50 (dd, J = 5.9, 3.6 Hz, 4H), 4.29 (dt, J = 16.6, 4.8 Hz, 9H), 4.05 (t, J = 4.7 Hz, 4H), 3.97 (q, J = 4.8 Hz, 8H), 3.78 (dd, J = 5.6, 3.6 Hz, 4H), 3.59 (dd, J = 5.6, 3.6 Hz, 4H), 3.39 (s, 6H). ^{13}C NMR (75 MHz, CDCl3) δ (ppm): 170.49, 163.07, 154.41, 154.39, 153.93, 151.29, 147.43, 146.76, 139.55, 134.78, 131.97, 128.93, 127.97, 126.87, 125.54, 125.31, 125.19, 124.16, 123.68, 122.48, 116.04, 114.83, 114.70, 105.88, 105.78, 97.58, 72.58, 70.99, 70.09, 69.96, 69.29, 68.12, 68.00, 65.57, 59.21. IR: ν_{max}/cm^{-1} 3061 (b, OH conj. acid) 2924 (b, –CH_2– glycol), 2217 (w, CN), 1713 (s, C=O ester) 1680 (m, C=O conj. acid). FD-MS (in MeCN) *m*/*z*: calculated for $C_{37}H_{69}N_3O_{16}S_2$ $[M]^+$: 1307.4119. Found: 1307.4095.

The ring [RING·4PF_6]

The ring was synthesized based on a protocol described in the literature with minor modifications.[34]

Compound **6** was combined with bromoxylene and the template in dry DMF and stirred for 30 days. After one night, a purple precipitate was observed. After 30 days the product was precipitated by the addition of ether. The purple solid was dissolved in 1 M NH_4Cl (50 mL) and to this, 50 mL of DCM was added. This mixture was heated at reflux under gentle stirring until the purple color disappeared. The DCM layer was separated from the water layer, after which the water layer was heated again at reflux with DCM. This was repeated two times until the purple color had disappeared completely. Upon addition of NH_4PF_6 to this water solution, a white precipitate was obtained. The solid was filtered and washed thoroughly with Milli-Q and ether. The product was obtained from recrystallization from acetonitrile. The ^{1}H NMR corresponds to the literature.[34]

Salt exchange [MV·2(PF_6)]. Methyl viologen dichloride (**MV·Cl_2**) (1.00 g; 7.78 mmol) was dissolved in Milli-Q water. To this, NH_4PF_6 was added as a solid until no more precipitation was observed. The white solid was filtered and washed thoroughly with Milli-Q and ether after which it was dried in a vacuum oven. The white solid was used without further purification.

Conflicts of interest

There are no conflicts to declare.

Acknowledgements

This study was supported by the Holland Research School for Molecular Sciences (HRSMC) and the University of Amsterdam. We would like to acknowledge Dr. Remko Detz and Lidy van der Burg for synthesizing the **P1** dye; Sandra Nurttila and René Becker for their help with the binding studies; and Prof. Dr S. Woutersen for fruitful discussions.

References

1 B. O'Regan and M. Grätzel, *Nature*, 1991, **353**, 737–740.
2 M. Freitag, J. Teuscher, Y. Saygili, X. Zhang, F. Giordano, P. Liska, J. Hua, S. M. Zakeeruddin, J. E. Moser, M. Grätzel and A. Hagfeldt, *Nat. Photonics*, 2017, **11**, 372–378.
3 B. P. Lechêne, M. Cowell, A. Pierre, J. W. Evans, P. K. Wright and A. C. Arias, *Nano Energy*, 2016, **26**, 631–640.
4 Y. Cui, C. Yang, H. Yao, J. Zhu, Y. Wang, G. Jia, F. Gao and J. Hou, *Adv. Mater.*, 2017, **29**, 1–7.
5 A. Hagfeldt, G. Boschloo, L. Sun, L. Kloo and H. Pettersson, *Chem. Rev.*, 2010, **110**, 6595–6663.
6 H. N. Tsao, C. Yi, T. Moehl, J. H. Yum, S. M. Zakeeruddin, M. K. Nazeeruddin and M. Grätzel, *ChemSusChem*, 2011, **4**, 591–594.
7 S. Mathew, A. Yella, P. Gao, R. Humphry-Baker, B. F. E. Curchod, N. Ashari-Astani, I. Tavernelli, U. Rothlisberger, M. K. Nazeeruddin and M. Grätzel, *Nat. Chem.*, 2014, **6**, 242–247.
8 K. Kakiage, Y. Aoyama, T. Yano, K. Oya, J. I. Fujisawa and M. Hanaya, *Chem. Commun.*, 2015, **51**, 15894–15897.
9 T. E. Rosser, M. A. Gross, Y. H. Lai and E. Reisner, *Chem. Sci.*, 2016, **7**, 4024–4035.
10 J. J. Leung, J. Warnan, D. H. Nam, J. Z. Zhang, J. Willkomm and E. Reisner, *Chem. Sci.*, 2017, **8**, 5172–5180.
11 F. Li, K. Fan, B. Xu, E. Gabrielsson, Q. Daniel, L. Li and L. Sun, *J. Am. Chem. Soc.*, 2015, **137**, 9153–9159.
12 J. He, H. Lindström, A. Hagfeldt and S. E. Lindquist, *Sol. Energy Mater. Sol. Cells*, 2000, **62**, 265–273.
13 N. Põldme, L. O'Reilly, I. Fletcher, J. Portoles, I. V. Sazanovich, M. Towrie, C. Long, J. G. Vos, M. T. Pryce and E. A. Gibson, *Chem. Sci.*, 2018, 20–22.
14 J. He, H. Lindström, A. Hagfeldt and S.-E. Lindquist, *J. Phys. Chem. B*, 1999, **103**, 8940–8943.

15 Z. Huang, G. Natu, Z. Ji, P. Hasin and Y. Wu, *J. Phys. Chem. C*, 2011, **115**, 25109–25114.
16 F. Odobel and Y. Pellegrin, *J. Phys. Chem. Lett.*, 2013, **4**, 2551–2564.
17 J. C. Freys, J. M. Gardner, L. D'Amario, A. M. Brown and L. Hammarström, *Dalton Trans.*, 2012, **41**, 13105–13111.
18 A. Morandeira, G. Boschloo, A. Hagfeldt and L. Hammarström, *J. Phys. Chem. B*, 2005, **109**, 19403–19410.
19 W. B. Swords, S. J. C. Simon, F. G. L. Parlane, R. K. Dean, C. W. Kellett, K. Hu, G. J. Meyer and C. P. Berlinguette, *Angew. Chem., Int. Ed.*, 2016, **55**, 5956–5960.
20 P. Qin, H. J. Zhu, T. Edvinsson, G. Boschloo, A. Hagfeldt and L. C. Sun, *J. Am. Chem. Soc.*, 2008, **130**, 17629.
21 A. Nattestad, A. J. Mozer, M. K. R. Fischer, Y. B. Cheng, A. Mishra, P. Bäuerle and U. Bach, *Nat. Mater.*, 2010, **9**, 31–35.
22 J. Preat, A. Hagfeldt and E. A. Perpète, *Energy Environ. Sci.*, 2011, **4**, 4537–4549.
23 S. Mori, S. Fukuda, S. Sumikura, Y. Takeda, Y. Tamaki, E. Suzuki and T. Abe, *J. Phys. Chem. C*, 2008, **112**, 16134–16139.
24 P. L. Anelli, P. R. Ashton, D. Philp, M. Pietraszkiewicz, M. V. Reddington, N. Spencer, J. F. Stoddart, C. Vicent, R. Ballardini, V. Balzani, M. T. Gandolfi, L. Prodi, M. Delgado, T. T. Goodnow, A. E. Kaifer, A. M. Z. Slawin and D. J. Williams, *J. Am. Chem. Soc.*, 1992, **114**, 193–218.
25 C. J. Wood, C. A. McGregor and E. A. Gibson, *ChemElectroChem*, 2016, **3**, 1827–1836.
26 P. R. Ashton, V. Balzani, O. Kocian, L. Prodi, N. Spencer and J. F. Stoddart, *J. Am. Chem. Soc.*, 1998, **120**, 11190–11191.
27 F. M. Raymo, K. N. Houk and J. F. Stoddart, *J. Org. Chem.*, 1998, **63**, 6523.
28 R. A. Bissell, E. Córdova, A. E. Kaifer and J. F. Stoddart, *Nat. Chem.*, 1994, **369**, 133–137.
29 J. W. Choi, A. H. Flood, D. W. Steuerman, S. Nygaard, A. B. Braunschweig, N. N. P. Moonen, B. W. Laursen, Y. Luo, E. Delonno, A. J. Peters, J. O. Jeppesen, K. Xu, J. F. Stoddart and J. R. Heath, *Chem.–Eur. J.*, 2006, **12**, 261–279.
30 H. Li, C. Cheng, P. R. McGonigal, A. C. Fahrenbach, M. Frasconi, W. G. Liu, Z. Zhu, Y. Zhao, C. Ke, J. Lei, R. M. Young, S. M. Dyar, D. T. Co, Y. W. Yang, Y. Y. Botros, W. A. Goddard, M. R. Wasielewski, R. D. Astumian and J. F. Stoddart, *J. Am. Chem. Soc.*, 2013, **135**, 18609–18620.
31 H. Li, A. C. Fahrenbach, A. Coskun, Z. Zhu, G. Barin, Y. L. Zhao, Y. Y. Botros, J. P. Sauvage and J. F. Stoddart, *Angew. Chem., Int. Ed.*, 2011, **50**, 6782–6788.
32 P. R. Ashton, R. Ballardini, V. Balzani, A. Credi, K. R. Dress, E. Ishow, C. J. Kleverlaan, O. Kocian, J. A. Preece, N. Spencer, J. F. Stoddart, M. Venturi and S. Wenger, *Chem.–Eur. J.*, 2000, **6**, 3558–3574.
33 P. Qin, M. Linder, T. Brinck, G. Boschloo, A. Hagfeldt and L. Sun, *Adv. Mater.*, 2009, **21**, 2993–2996.
34 M. Asakawa, W. Dehaen, G. L'abbé, S. Menzer, J. Nouwen, F. M. Raymo, J. F. Stoddart and D. J. Williams, *J. Org. Chem.*, 1996, **61**, 9591–9595.
35 M. Venturi, S. Dumas, V. Balzani, J. Cao and J. F. Stoddart, *New J. Chem.*, 2004, **28**, 1032–1037.
36 C. A. Hunter and H. L. Anderson, *Angew. Chem., Int. Ed.*, 2009, **48**, 7488–7499.
37 R. Castro, K. R. Nixon, J. D. Evanseck and A. E. Kaifer, *J. Org. Chem.*, 1996, **61**, 7298–7303.

38 M. Jonsson, A. Houmam, G. Jocys and D. D. M. Wayner, *J. Chem. Soc., Perkin Trans. 2*, 1999, **117**, 425–429.
39 P. R. Ashton, L. Pérez-García, J. F. Stoddart, R. Ballardini, V. Balzani, A. Credi, M. T. Gandolfi, L. Prodi, M. Venturi, S. Menzer, A. J. P. White and D. J. Williams, *J. Am. Chem. Soc.*, 1995, **117**, 11171–11197.
40 A. Yella, S. Mathew, S. Aghazada, P. Comte, M. Grätzel and M. K. Nazeeruddin, *J. Mater. Chem. C*, 2017, **5**, 2833–2843.
41 J. J. Nelson, T. J. Amick and C. M. Elliott, *J. Phys. Chem. C*, 2008, **112**, 18255–18263.
42 T. Larsson, M. Wedborg and D. Turner, *Anal. Chim. Acta*, 2007, **583**, 357–363.
43 X. Wang, S. S. Nurttila, W. I. Dzik, R. Becker, J. Rodgers and J. N. H. Reek, *Chem.–Eur. J.*, 2017, **23**, 14769–14777.

